RSC Advances

PAPER

View Article Online
View Journal | View Issue

Cite this: *RSC Adv.*, 2015, **5**, 57847

A SERS study of oxidation of glutathione under plasma irradiation†

Shanshan Ma[a] and Qing Huang*[ab]

This paper reports a new application of surface enhanced Raman scattering (SERS) in analysis of oxidation of glutathione (GSH) to oxidized glutathione (GSSG), an important biochemical redox reaction in biological systems, under oxidative stress imposed by dielectric barrier discharge (DBD). Using the silver nanoparticles (NPs) prepared through the reduction of $AgNO_3$ by beta-cyclodextrin (β-CD), the transformation of GSH to GSSG under DBD irradiation can be probed with only a small quantity of sample at low concentration. Based on the intensity ratio of two characteristic Raman bands, *i.e.*, the band at 1051 cm^{-1} (C–N stretching) and the band at 509 cm^{-1} (S–S stretching), which stem respectively from GSH and GSSG, the conversion between the reduced and oxidized glutathione can be determined quantitatively. This work demonstrates another useful extension of the SERS technique applied to bioscience research, *i.e.*, rapid probing and quantitative assessing of chemical reactions of biomolecules under oxidative stress conditions.

Received 24th April 2015
Accepted 24th June 2015

DOI: 10.1039/c5ra07440a

www.rsc.org/advances

Introduction

Because of the advantages of high sensitivity and fingerprint character, surface-enhanced Raman spectroscopy (SERS) has become a very powerful analytical tool which has been successfully applied in many diversified fields.[1–5] Especially, there is an increasing interest in application of this technique in bioscience research. For example, SERS has been applied in the rapid trace-detection of biomolecules, such as DNA[6,7] and proteins,[8–11] and also sensitive identification of intrinsic cancer biomarkers in cells.[12]

However, up to now there are very few reports in the literature concerning the application of SERS in the research of radiation-biological field, although different kinds of radiations exist ubiquitously and can induce abundant biological effects.[13] For ionizing radiation, it possesses the energy that can break up water molecules and give rise to reactive oxygen species (ROS), which may subsequently induce complex reactions of biomolecules[14–16] and cause cell injury or cell death.[17] Although conventional analytical tools such as chromatography and mass spectrometry can be utilized to investigate the involved reactions, they are normally time-consuming and expensive in operation, and moreover, they cannot render direct and *in situ* measurement of the involved chemical processes, not to mention the real-time measurement in living cells.

In this sense, SERS just provides the capability of quick and trace chemical analysis, and therefore, it is intriguing for us to introduce SERS and test its applicability in the radiation-biological studies. Previously, Ou *et al.* have applied SERS for DNA analysis in the nasopharyngeal carcinoma cells under X-ray radiation.[18] Also, we have employed SERS to study the chemical reactions of tyrosine, a small biomolecule, under particle irradiation (including plasma and electron-beam irradiations).[19] In this work, we intended to make use of SERS to probe the ROS induced reaction of glutathione (GSH), a peptide that is composed of three amino acid residue, namely, glutamine, cysteine and glycine. This biomolecule is an important anti-oxidant in living organisms, and it is the most prevalent cellular thiol involved in major biologic processes.[20,21] The depletion of GSH in cell would result in the mitochondria impairment[22] or apoptosis.[23] The thiol of GSH is reactive, and can easily be converted into oxidized glutathione (GSSG), the major product of GSH oxidation.[24] On the other hand, GSSG can also be reduced to GSH by reductase. In cellular redox reactions, keeping an optimal GSH and GSSG ratio is crucial to cell survival.[21] Breakdown of the balance between GSH and GSSG upon exposure of ROS can result in protein damage and apoptosis.[21]

$$\mathrm{GSH} \xrightarrow{\mathrm{ROS}} \mathrm{GS}^{\cdot}$$

$$\mathrm{GS}^{\cdot} \xrightarrow[\text{or } \mathrm{GS}^{\cdot}]{\mathrm{GSH}} \mathrm{GS-SG}$$

To mimic low-energy particle irradiation induced oxidative stress, we employed dielectric barrier discharge (DBD), an

[a]*Key Laboratory of Ion Beam Bio-engineering, Institute of Technical Biology and Agriculture Engineering, Hefei Institutes of Physical Science, Chinese Academy of Sciences, Hefei, 230031, Anhui Province, PR China. E-mail: huangq@ipp.ac.cn*

[b]*University of Science & Technology of China, Hefei, Anhui 230026, People's Republic of China*

† Electronic supplementary information (ESI) available. See DOI: 10.1039/c5ra07440a

emerging non-thermal plasma technique which is regarded as one of advanced oxidation processes (AOPs).[25,26] During plasma discharge, energetic particles including electrons and ions are produced, together with the plasma induced ROS such as hydrogen peroxide and hydroxyl radicals.[27] As for the SERS measurements, we employed Ag nanoparticles (Ag NPs) which were synthesized through reduction of $AgNO_3$ by beta-cyclodextrin (β-CD) under alkaline condition. We then probed the damage of GSH and production of GSSG based on SERS, and due to careful spectral analysis we could make quantitative assessment of conversion between GSH and GSSG under oxidative stress.

Experiments

Materials and reagents

Silver nitrate ($AgNO_3$), catalase (CAT) were obtained from Sigma-Aldrich Co, Ltd. Glutathione (GSH), oxidized glutathione (GSSG), beta-cyclodextrin (β-CD), methyl alcohol were purchased from Sangon Biotech (Shanghai) Co. Potassium phosphate monobasic (KH_2PO_4) and phosphoric acid were purchased from Sinopharm Chemical Reagent Co., Ltd. All the chemicals were of analytical grade and used as received without any further purification.

Non-thermal plasma irradiation

To generate reactive oxygen species (ROS), non-thermal plasma irradiation was employed. Fig. 1 shows the schematic plot of our set-up of dielectric barrier discharge (DBD). Briefly, two stainless steel plates were used as the electrodes, in which the upper one was connected to the power supply and the other one was connected to the ground. A circular quartz container covered by a quartz plate was placed between the electrodes. The discharge argon gas was introduced into the reactor and the plasma discharge was formed in the gas–solution interface. The applied voltage was about 16 kV, and when the discharge was steady, the current was about 1 mA. For the DBD irradiation experiment, 4 mL 5 mM GSH solution was injected into the reactor, followed by plasma irradiation. After the discharge treatment, the solution was removed from the reactor, and treated with catalase to deplete the surplus hydrogen peroxide in the solution.

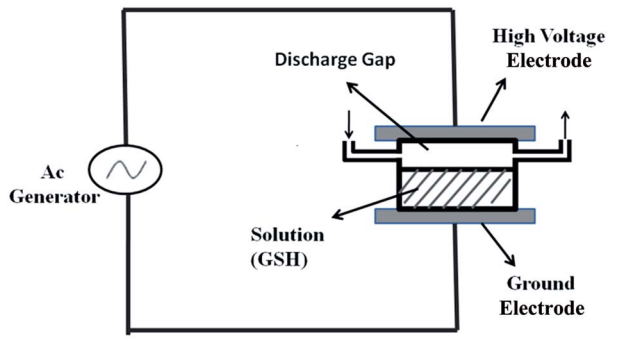

Fig. 1 The schematic plot of the DBD set-up. For the atmospheric non-thermal discharge, argon gas was filled in the container, and the discharge voltage was about 16 kV with the current about 1 mA. The volume of the solution sample was 4 mL.

Preparation of silver colloids

The Ag nanoparticles were synthesized through the reduction of $AgNO_3$ (0.6 mM) by β-CD under alkaline condition. Considering the low solubility of β-CD in water (7 mM), the reaction solution was heated at 80 °C. The overall reaction took for 10 min, and the final silver solution showed a yellow color. All the glass or quartz container were cleaned by aqua regia (HNO_3 : HCl = 1 : 3) and piranha solution (H_2O_2 : H_2SO_4 = 1 : 3), followed by washing with deionized water.

UV-vis absorption and SEM measurements

In order to characterize the silver colloids prepared under different conditions, UV-vis spectroscopy and scanning electron microscope (SEM) were employed. The UV-visible absorption property was examined using UV-vis spectrometer (SHIMADZH UV-2550). The images of the silver NPs were provided by scanning electron microscope (SEM) with a Hitachi S-4800 machine (SEM, SIRION 200, Toshiba S4800).

SERS measurements and spectral analysis

For SERS detection, the silver colloid solution was added to 20 μL GSH/GSSG samples. Then 5 μL of the mixture was dropped onto the quartz plate, and dried under room temperature. The SERS spectra were recorded using HORIBA JOBIN YVON XploRA Raman Spectrometer equipped and a 50× objective. All the Raman spectra were excited with 785 nm laser of power about 0.2 mW focused on the samples. The laser focus spot size was about 2 μm in diameter, and the acquisition time for an individual Raman spectrum was typically 10 s.

High performance liquid chromatography (HPLC) measurement

The HPLC was carried using the instrument Waters-600E equipped with the chromatographic column RP-C18 column. Mobile phase was the mixture of 0.05 M KH_2PO_4 (phosphoric acid was added to keep the pH 3) and methyl alcohol, with the volume ratio as 97 : 3. The flow rate was 1 mL min^{-1} and the column temperature was 30 °C, while the detection wavelength was 210 nm.

Results and discussion

Characterization of Ag NPs

Ag NPs were prepared by reduction of $AgNO_3$ with β-CD, a substance which has medium reduction ability under the alkaline condition. β-CD is cyclic oligosaccharides and the interior cavity of CD is relatively hydrophobic while the external cavity is hydrophobic, it has been used for synthesis of Au nanoparticles[28] and Ag shell on the Au surface[29] previously. Fig. 2 shows the SEM images of the as-prepared Ag nanoparticles (NPs), showing that the morphology of Ag NPs is spherical and the quite uniform with the indicated diameter *ca.*

40 nm. The surface plasmon resonance (SPR) peak of the Ag NPs is about at 406 nm, and the zeta potential measurement demonstrates that the Ag NPs are homogeneously negatively-charged and so the colloids were dispersed well without aggregation for the concentrations used in this work (Fig. S1†).

The SERS activity of the Ag NPs was checked by using the standard R6G. The lower detect limitation is 10^{-11} M, and accordingly, the enhancement factors (EFs) is about 5×10^6 (Fig. S2, ESI Part 1†).

In this work we employed the Ag NPs for SERS analysis of GSH/GSSG because we found that they were very suitable for our biomolecular study. Compared with Ag NPs obtained by others methods, these Ag NPs had very low background signals, resulting in little interference to the detection of the biomolecules.

SERS identification of GSH and GSSG

The conventional analysis of GSH and GSSG can be achieved by colorimetric tests using GSH/GSSG assay kits or by HPLC based on the derivation of thiol group, which however requires bulk volume samples. Also, for conventional Raman spectroscopy, although the GSH concentration in realistic bio-samples may reach millimolar (0.5–10 mM),[30] it also requires bulk volume of samples and the normal Raman signal of GSH is still too weak to be clearly determined. Therefore, it is critical to improve the Raman detection sensitivity, and SERS can greatly amplify the Raman signal and thus provide the solution (Fig. S3a†). Based on SERS technique, only a tiny volume of sample (5 μL) was enough for our purpose of examination.

To achieve both qualitative and quantitative analysis, at first the SERS spectra of pure GSH and GSSG were recorded, with which we can therefore readily identify the mixture of GSH/GSSG in the DBD treated samples. The typical SERS spectra are shown in Fig. 3 and the assignments are shown in Table 1. For the assignment of Raman bands in SERS spectra, we also conducted normal Raman measurements for comparison (Fig. S4†) and noticed that Raman spectra could be influenced by many other factors under different under different conditions.[31,32] Also, we were ensured that the SERS measurements were reproducible (Fig. S3b†). For the spectra of GSH and GSSG, the most prominent band occurs at 657 cm^{-1} and 659 cm^{-1}, respectively, which is attributed to the C–S stretching vibration.[33] Fortunately, this C–S vibration has almost the identical Raman intensity for both GSH and GSSG per unit molar (Fig. S8†), so we can use this band as an internal reference for normalization of the spectra, and as will be explained in the following section, this property can also facilitate us to give the quantitative evaluation of the GSH/GSSG mixture samples. For identification of GSSG, the characteristic band appears at 509 cm^{-1}, which stems from the –S–S– stretching vibration,[34,35] and this band can be utilized as the unique signature for analysis of GSSG. To discriminate GSH, the strong signal at 1051 cm^{-1} can be identified, which is ascribed to the C–N stretching vibration. To be noted, the same vibration band for GSSG appears at 1048 cm^{-1}, which is however much weaker in intensity. The Raman intensity at 1051 cm^{-1} for GSH is about 6–7 folds stronger than that of the 1048 cm^{-1} band for GSSG (Fig. S7†), suggesting that we can utilize this 1051 cm^{-1} band as the characteristic band for quantitative evaluation of GSH. Also, in the evaluation of GSH/GSSG mixture samples, the signal at 1048 cm^{-1} can be neglected for the estimation of the intensity at 1051 cm^{-1} for GSH.

Based on the above-approved characteristic bands for GSH and GSSG, the quantities of GSH/GSSG in the mixture samples can be evaluated. For this purpose, it also requires to measure the standard curves for the SERS intensity *versus* concentration of GSH (Fig. 4(a)), and also, in order to avoid the uncertainty in determining the absolute SERS intensity, it is favorable to use the relative parameters such as the intensity ratio of the 509 cm^{-1} band to the 1051 cm^{-1} band for estimating the GSH/GSSG contents in the DBD-treated samples. The standard curves for determining the concentration of C_{GSH} and the concentration

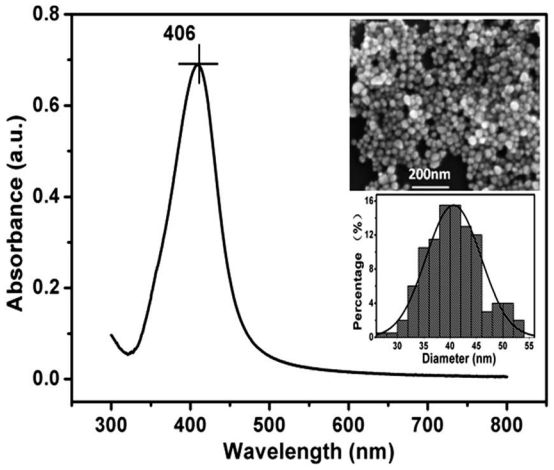

Fig. 2 The absorption spectrum of the silver colloids, showing the absorption maximum at 406 nm. Inset: the SEM picture (above) and the size analysis of the Ag NPs (below), showing the average diameter about 40 nm.

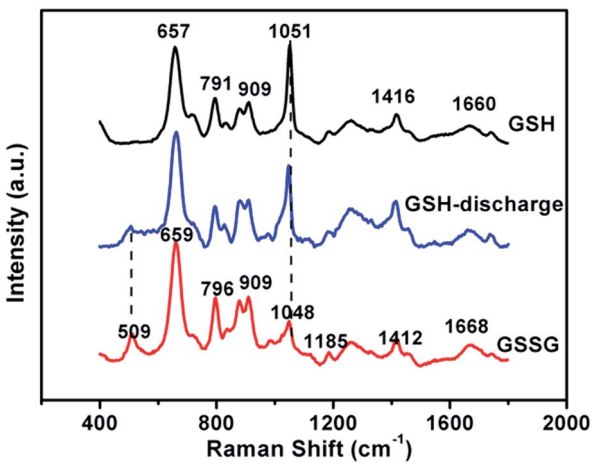

Fig. 3 The SERS spectra of GSH, GSSG and DBD-treated samples. The assignments of the bands are given in Table 1.

Table 1 The wavenumbers (cm^{-1}) and the assignments of the observed SERS bands for GSH and GSSG

GSH	GSSG	Assignment
	509	S–S[35]
657	659	C–S stretching[36]
791	796	Amide V[36]
909	909	C–C stretching[36]
1051	1048	C–N stretching[36]
1416	1412	–COO-symmetric stretching[36]
1660	1668	Amide I[36]

ratio of C_{GSSG}/C_{GSH} are shown in Fig. 4(b). Here we prepared the GSH/GSSG mixture calibration samples with known contention ratios, with C_{GSH} in the range of 10^{-5} to 10^{-4} M, and C_{GSSG} in the range of 10^{-5} to 4.5×10^{-5} M. The intensity ratio between the band at 509 cm^{-1} and 1051 cm^{-1} increases with the concentration ratio of C_{GSSG}/C_{GSH}. Based on the standard curves provided by Fig. 4, we can estimate the loss of GSH and the production of GSSG under the oxidative stress imposed by DBD irradiation.

Then, we measured the intensity ratios for the DBD treated samples, and the result is shown in Fig. 5. The inset presents the SERS spectra which show clearly the intensity decrease for the 1051 cm^{-1} band and the increase for the 509 cm^{-1} band, confirming the loss of GSH and the formation of GSSG under the DBD irradiation.

For the quantitative evaluation of the SERS spectra, some notes should be taken. First, DBD produces hydrogen peroxide which displays an adverse effect on the SERS detection because it can interact with silver colloids and affect the stability of Ag NPs.[37,38] To circumvent this problem we added catalase to remove the residual H_2O_2. Second, the SERS measurement could also be affected by the pH change caused by DBD treatment. So we checked that the pH value of the DBD treated GSH solution, and found that the pH value was changed from 4.8 (initial pH value without DBD treatment) to 2.7 (10 min of DBD treatment). Fortunately, within this range, the SERS intensity was only slightly varied (Fig. S5†), therefore the pH effect could be ignored in our case. Third, another difficulty for quantitative evaluation was that the SERS intensity was also dependent on the quantity of Ag NPs applied. To overcome the uncertainty and ensure the reproducibility of the measurement, we checked the SERS signals using different concentration of Ag NPs. It was found that when sufficient amount of Ag NPs relative to the low concentration of GSH (in the range of 10^{-4}) was applied, the SERS signal from GSH was relatively unchanged (Fig. S6a†); as for assessment of GSSG, when its concentration was low or comparable with that of GSH, which was true for our case, the small discrepancy among the different calibration curves obtained for different silver colloid concentration could be neglected (Fig. 4(b)). Therefore, in our SERS experiment we applied an optimal concentration of 2 nM of silver colloids, and ensured that this same condition was applied for all the SERS measurements. As a result, our measurements were reproducible and reliable for the quantitative assessment.

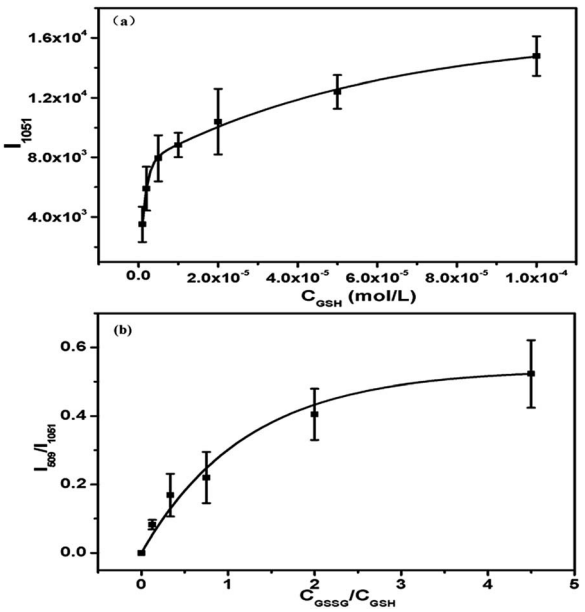

Fig. 4 (a) The standard curve of SERS intensity of the 1051 cm^{-1} band (I_{1051}) *versus* the concentration of GSH (C_{GSH}). (b) The standard curve for evaluation of the GSH/GSSG mixture based on the intensity ratio of the 509 cm^{-1} band of GSSG to the 1051 cm^{-1} band of GSH.

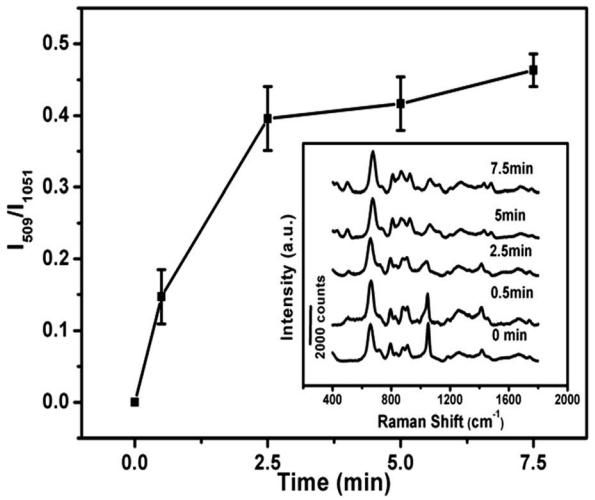

Fig. 5 The SERS intensity ratio of I_{509}/I_{1051} *versus* the DBD irradiation time. Inset: the SERS spectra of the DBD treated samples. All the data points are statistical averages of at least three measurements.

Determination of GSH/GSSG conversion

As described previously, the discharge plasma can produce ROS which leads to the transformation from GSH to oxidized form GSSG. With the aid of the standard curves in Fig. 4, and based on the SERS intensity ratios given by Fig. 5, we can estimate contents of GSH and GSSG. The result is shown in Fig. 6, where C_{GSH} was obtained using the standard curve in Fig. 4(a), while C_{GSSG} was obtained from C_{GSH} and according to

the standard curve regarding the C_{GSSG}/C_{GSH} in Fig. 4(b). Moreover, in order to confirm the accuracy of SERS, other methods could be employed. In our previous work, the quantitative analysis of GSH and GSSG was achieved by using GSH and GSSG assay kits.[39] Herein HPLC was employed to measure GSH and GSSG (Fig. S9†). As seen in Fig. 6, the result of SERS agrees well with the HPLC result, confirming the applicability of SERS for the reliable quantitative evaluation of GSH/GSSG transformation.

Furthermore, the conversion percentage can be obtained according to the following formula:

$$X = \frac{2 \times C_{GSSG}}{(C_0 - C_{GSH})} \times 100\% \quad (1)$$

where C_0 refers to the initial concentration of GSH. Since one GSSG molecule comes from combination of two GSH molecules, when GSH is completely converted to GSSG, X is 100%. To estimate the conversion efficiency in the real case, we measured the ratios of the SERS intensity of S–S and C–S bands (Fig. S8†), and calculated X according to the following equation:

$$X = \frac{2P \times C_{GSH}}{(P^o - P) \times (C_0 - C_{GSH})} \times 100\% \quad (2)$$

where P is defined as I_{509}/I_{659} for the SERS measurements, and P^o is a constant ratio per unit molar (ESI Part 5†). The derivation of eqn (2) is given in the ESI-Part S4.† Fig. 7 shows the result evaluated from the SERS data according to eqn (2). As illustrated by Fig. 7, about 70%–90% of GSH can be converted to GSSG under the DBD irradiation. This result is in good agreement of the evaluation obtained from the HPLC measurement.

Formerly, our group have applied DC glow discharge plasma, another form of plasma to mimic the oxidative stress on GSH, and applied conventional Raman spectroscopy to detect the conversion between GSH and GSSG.[40] Compared to the result obtained from the DC glow discharge, the DBD-induced damage of GSH is smaller and the conversion efficiency is higher. This is mainly because that the DC glow discharge gives rise to higher amount of hydroxyl radical as well as higher ratio

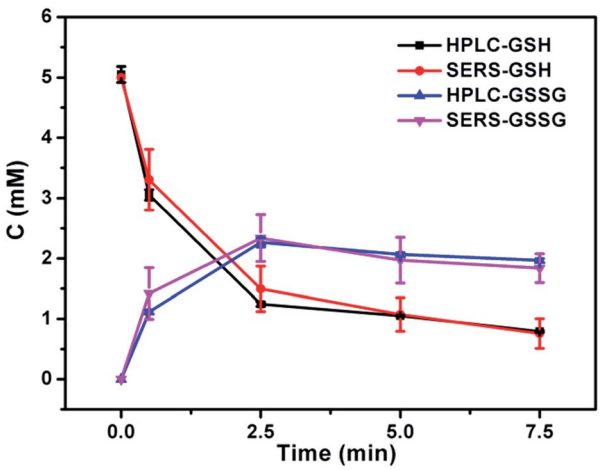

Fig. 6 The comparison in evaluation of the GSH and GSSG contents between the SERS result and the HPLC result.

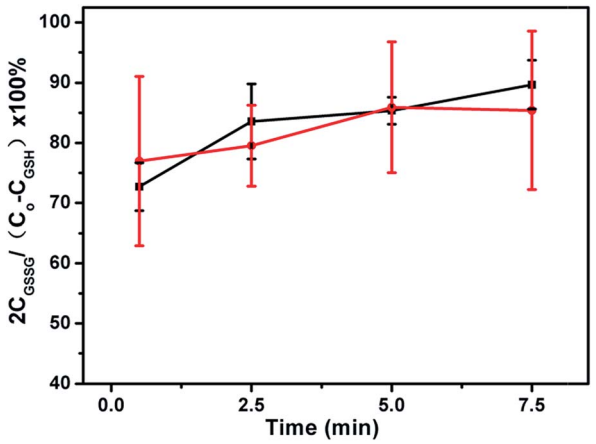

Fig. 7 The transformation efficiencies for the GSH/GSSG redox reaction, assessed from both the SERS measurement and the HPLC measurement.

of hydroxyl radical to hydrogen peroxide,[41] which brings more severe damage to GSH, so that less GSH can be converted to GSSG. In addition, for the detection method, compared to our previous work,[40] here we employed SERS rather than normal Raman for the measurement, the sensitivity has been improved more than 10^3 times. In that way, we could achieve detection of trace amount of GSH and GSSG at low concentration. This is an important advance because it gives us the possibility to monitor the redox reaction rapidly in cells.

Conclusions

Presently, SERS has become an intensively explored and powerful tool in analytical chemistry, and there is an increasing interest for employing SERS to probe or monitor biochemical reactions in biological systems.[42,43] However, one of big challenges is to identify different mixtures quantitatively in the reaction system. Our work is certainly an effort in this regard. In this work, we have synthesized silver nanoparticles through the reduction of $AgNO_3$ by β-CD under the alkaline condition, and employed these Ag NPs to achieve sensitive and quantitative SERS analysis of the redox reaction of GSH/GSSG transformation under oxidative stress imposed by non-thermal plasma DBD irradiation. Based on the characteristic bands of 509 and 1051 cm^{-1} for GSSG and GSH respectively, we could analyze the mixture of GSH and GSSG simultaneously and make the quantitative distinction and evaluation of conversion between GSH and GSSG conveniently and quickly. As such, we have not only successfully employed the method SERS for evaluating the mixture of GSH/GSSG quantitatively, but also introduced it in the study of radiation chemistry involving redox reaction of biomolecules. Because GSH/GSSG redox reaction is a most important process in biological systems, and employment of SERS improves the detection sensitivity tremendously, this work therefore also suggests the potential applicability of SERS in the radiobiological study of cells against oxidative stress.

Acknowledgements

This work was financially supported by the National Basic Research Program of China (Grant No. 2013CB934304), the National natural Science Foundation of China (Grant No. 11175204, 11475217) and the Cross-disciplinary Collaborative Teams Program of CAS.

Notes and references

1 J. F. Li, Y. F. Huang and Y. Ding, *Nature*, 2010, **464**, 392.
2 A. Campion and P. Kambhampati, *Chem. Soc. Rev.*, 1998, **27**, 241.
3 K. Hering, D. Cialla and K. Ackermann, *Anal. Bioanal. Chem.*, 2008, **39**, 113.
4 Y. Lu, Q. Huang and G. Meng, *Analyst*, 2014, **139**, 3083.
5 C. Zhu, G. Meng and Q. Huang, *J. Hazard. Mater.*, 2012, **211**, 389.
6 K. Kneipp, H. Kneipp and V. B. Kartha, *Phys. Rev. E: Stat. Phys., Plasmas, Fluids, Relat. Interdiscip. Top.*, 1998, **57**, R6281.
7 A. Barhoumi, D. Zhang and F. Tam, *J. Am. Chem. Soc.*, 2008, **130**, 5523.
8 I. Delfino, A. R. Bizzarri and S. Cannistraro, *Biophys. Chem.*, 2005, **113**, 41.
9 H. Xu, E. J. Bjerneld and M. Käll, *Phys. Rev. Lett.*, 1999, **83**, 4357.
10 E. J. Bjerneld, Z. Földes-Papp and M. Käll, *J. Phys. Chem. B*, 2002, **106**, 1213.
11 S. K. Deb, B. Davis and G. M. Knudsen, *J. Am. Chem. Soc.*, 2008, **130**, 9624.
12 U. S. Dinish, G. Balasundaram and Y. T. Chang, *Sci. Rep.*, 2014, **4**, 4075.
13 (*a*) U.N.S.C.o.t.E.o.A, United Nations Pubns, 1986; (*b*) J. Haywood and O. Boucher, *Rev. Geophys.*, 2000, **38**, 513–543.
14 J. F. Ward, *Prog. Nucleic Acid Res. Mol. Biol.*, 1988, **35**, 95.
15 G. F. Vile and R. M. Tyrrell, *Free Radicals Biol. Med.*, 1995, **18**, 721.
16 V. Borshchevskiy, E. Round and I. Erofeev, *Acta Crystallogr., Sect. D: Biol. Crystallogr.*, 2014, **70**, 2675.
17 J. S. Russell, W. Burgan and K. A. Oswald, *Clin. Cancer Res.*, 2003, **9**, 3749.
18 L. Ou, Y. Chen and Y. Su, *J. Raman Spectrosc.*, 2013, **44**, 680.
19 J. Zhang, Q. Huang and G. Yao, *J. Mol. Struct.*, 2014, **1072**, 195.
20 H. Sies, *Free Radicals Biol. Med.*, 1999, **27**, 916.
21 D. M. Townsend, K. D. Tew and H. Tapiero, *Biomed. Pharmacother.*, 2003, **57**, 145.
22 M. Merad-Boudia, A. Nicole and D. Santiard-Baron, *Biochem. Pharmacol.*, 1998, **56**, 645.
23 R. Franco, M. I. Panayiotidis and J. A. Cidlowski, *J. Biol. Chem.*, 2007, **282**, 30452.
24 M. Tamba and A. Torreggiani, *Res. Chem. Intermed.*, 2002, **28**, 57.
25 V. K. Sharma, T. M. Triantis and M. G. Antoniou, *Sep. Purif. Technol.*, 2012, **91**, 3.
26 H. Zhang, Q. Huang and Z. Ke, *Water Res.*, 2012, **46**, 6554.
27 K. P. Arjunan, G. Friedman and A. Fridman, *J. R. Soc., Interface*, 2012, **9**, 2447.
28 T. Huang, F. Meng and L. Qi, *Langmuir*, 2009, **26**, 7582.
29 Y. Lu, G. Yao and K. Sun, *Phys. Chem. Chem. Phys.*, 2014, DOI: 10.1039/c4cp04904g.
30 A. Meister and M. E. Anderson, *Annu. Rev. Biochem.*, 1983, **52**, 711.
31 P. Sahoo, P. S. Murthy and S. Dhara, *et al.*, *J. Nanopart. Res.*, 2013, **15**, 1841.
32 S. Sengupta, N. Maiti and R. Chadha, *et al.*, *Chem. Phys.*, 2014, **436**, 55.
33 M. Lv, H. Gu and X. Yuan, *J. Mol. Struct.*, 2012, **1029**, 75.
34 E. López-Tobar, B. Hernández and M. Ghomi, *J. Phys. Chem. C*, 2013, **117**, 1531.
35 C. David, S. Foley and M. Enescu, *Phys. Chem. Chem. Phys.*, 2009, **11**, 2532.
36 G. G. Huang, X. X. Han and M. K. Hossain, *Anal. Chem.*, 2009, **81**, 5881.
37 D. He, S. Garg and T. D. Waite, *Langmuir*, 2012, **28**, 10266.
38 D. He, A. M. Jones and S. Garg, *J. Phys. Chem. C*, 2011, **115**, 5461.
39 J. Liu, Z. Qi and Q. Huang, *et al.*, *J. Mol. Struct.*, 2013, **1031**, 1.
40 Z. Ke, Z. Yu and Q. Huang, *Plasma Processes Polym.*, 2013, **10**, 181.
41 H. Zhang, L. Yang and Z. Yu, *J. Hazard. Mater.*, 2014, **268**, 33.
42 G. Xue, Q. Dai and S. Jiang, *J. Am. Chem. Soc.*, 1988, **110**, 2393–2395.
43 W. Xie, B. Walkenfort and S. Schluecker, *J. Am. Chem. Soc.*, 2013, **135**, 1657.

